

Electronic Supplementary Information

Shape-controlled synthesis of $\text{Cu}_{31}\text{S}_{16}$ -metal sulfide heteronanostructures *via* a two-phase approach

Miao Wang,^a Aiwei Tang,^{*ab} Lan Peng,^{ab} Chunhe Yang^a and Feng Teng^{*b}

^a*Department of Chemistry, School of Science, Beijing JiaoTong University, Beijing 100044, PR China. E-mail: awtang@bjtu.edu.cn; Tel: +86 10 51683627*

^b*Key Laboratory of Luminescence and Optical Information, Ministry of Education, Beijing JiaoTong University, Beijing 100044, PR China. E-mail: fteng@bjtu.edu.cn*

Experimental details

Synthesis of $\text{Cu}_{31}\text{S}_{16}$ -ZnS HNS

In a typical synthesis of icecream-like $\text{Cu}_{31}\text{S}_{16}$ -ZnS HNS, 0.5 mmol of $\text{Cu}(\text{NO}_3)_2 \cdot 3\text{H}_2\text{O}$ and 1 mmol of $\text{Zn}(\text{NO}_3)_2 \cdot 2\text{H}_2\text{O}$ were added into 20 mL of deionized water. After keeping stirring for 15 min, the clear solution was transferred to a 50 mL of Teflon-lined autoclave, following by addition of 3 mL DDT. As a result, a two-phase reaction system was formed, in which DDT is the upper organic phase, and the DDT acts as not only the sulfur source but also as a surface-capping agent and reducer. The lower phase is the aqueous solution, which consists of the metal salts. Finally, the Teflon-lined autoclave was sealed and maintained at 190 °C for 20 h. After the reaction was finished, the autoclave was cooled naturally to room temperature. The products were collected by adding ethanol and centrifugation at 6000 rpm for 10 min. The precipitation was then re-dispersed in chloroform and collected by adding ethanol and centrifugation. The purification process was repeated three times. Finally the products were dispersed in chloroform or dried in vacuum for further characterization. In order to study the effects of the molar ratios of Zn/Cu precursors on the morphology and crystal structure of the as-obtained HNS, the control experiments were performed based on the same process except 0.25 mmol and 0.5 mmol of $\text{Zn}(\text{NO}_3)_2 \cdot 2\text{H}_2\text{O}$ were used. Thus, different-shaped $\text{Cu}_{31}\text{S}_{16}$ -ZnS HNS s were synthesized by using different molar ratios of Cu/Zn precursors of 2:1, 1:1 and 1:2. To study the formation mechanism of

different-shaped $\text{Cu}_{31}\text{S}_{16}\text{-ZnS}$ HNS, a series of matchstick-like and icecream-like $\text{Cu}_{31}\text{S}_{16}\text{-ZnS}$ HNS have been synthesized by varying the reaction time, such 5, 10 and 15 h. To confirm the formation of $\text{Cu}_{31}\text{S}_{16}$ phase, the sample was synthesized without Zn precursors while other reaction conditions were kept the same as the synthesis of $\text{Cu}_{31}\text{S}_{16}\text{-ZnS}$ HNS.

Additionally, to study the effects of zinc sources on the formation of $\text{Cu}_{31}\text{S}_{16}\text{-ZnS}$ HNS, different zinc sources including ZnAc_2 , ZnSO_4 and ZnCl_2 were employed to replace $\text{Zn}(\text{NO}_3)_2$ while other reaction conditions were kept the same as that of the synthesis of icecream-like HNS.

Synthesis of $\text{Cu}_{31}\text{S}_{16}\text{-CdS}$ HNS

A typical synthesis of waterdrop-like $\text{Cu}_{31}\text{S}_{16}\text{-CdS}$ HNS is described as follows: 0.5 mmol of $\text{Cu}(\text{NO}_3)_2 \cdot 3\text{H}_2\text{O}$ and 0.25 mmol of $\text{Cd}(\text{NO}_3)_2 \cdot 2\text{H}_2\text{O}$ were added into 20 mL of deionized water, then transferred to a 50 mL of Teflon-lined autoclave, following by addition of 3 mL DDT. Other reaction conditions were kept the same as that of synthesis of icecream-like $\text{Cu}_{31}\text{S}_{16}\text{-ZnS}$ HNS. To study the effects of the molar ratios of Cu/Cd precursors on the morphology and crystal structure of the as-obtained HNS, 0.75 mmol of $\text{Cd}(\text{NO}_3)_2 \cdot 2\text{H}_2\text{O}$ was used as Cd sources while other reaction conditions were kept the same as above.

Synthesis of $\text{Cu}_{31}\text{S}_{16}\text{-CuInS}_2$ HNS

For the synthesis of matchstick-like $\text{Cu}_{31}\text{S}_{16}\text{-CuInS}_2$ HNS, 0.5 mmol of $\text{In}(\text{NO}_3)_3$ and 0.5 mmol of $\text{Cu}(\text{NO}_3)_2 \cdot 3\text{H}_2\text{O}$ were used as the In and Cu sources, and other reaction conditions were kept the same as that of synthesis of icecream-like $\text{Cu}_{31}\text{S}_{16}\text{-ZnS}$ HNS.

Characterizations

Transmission electron microscopy (TEM) observations were taken on a Hitachi-7650 TEM with an acceleration voltage of 100 kV. The high-resolution TEM (HRTEM) images were taken on a JEM-2010 at an accelerating voltage of 200 kV. Powder X-ray diffraction (XRD) patterns were recorded by a Bruker D8 Discover X-ray Diffractometer with a Cu $\text{K}\alpha$ radiation source ($\lambda=1.54056$ Å). X-Ray photoelectron spectroscopy (XPS) measurement was collected on Thermo ESCALAB 250Xi XPS spectrometer using non-monochromatic Al $\text{K}\alpha$ (1486.6 eV). UV-Vis-NIR absorption spectra were recorded using a Varian 5000 spectrophotometer. All of the measurements were performed at room temperature.

Figure. S1

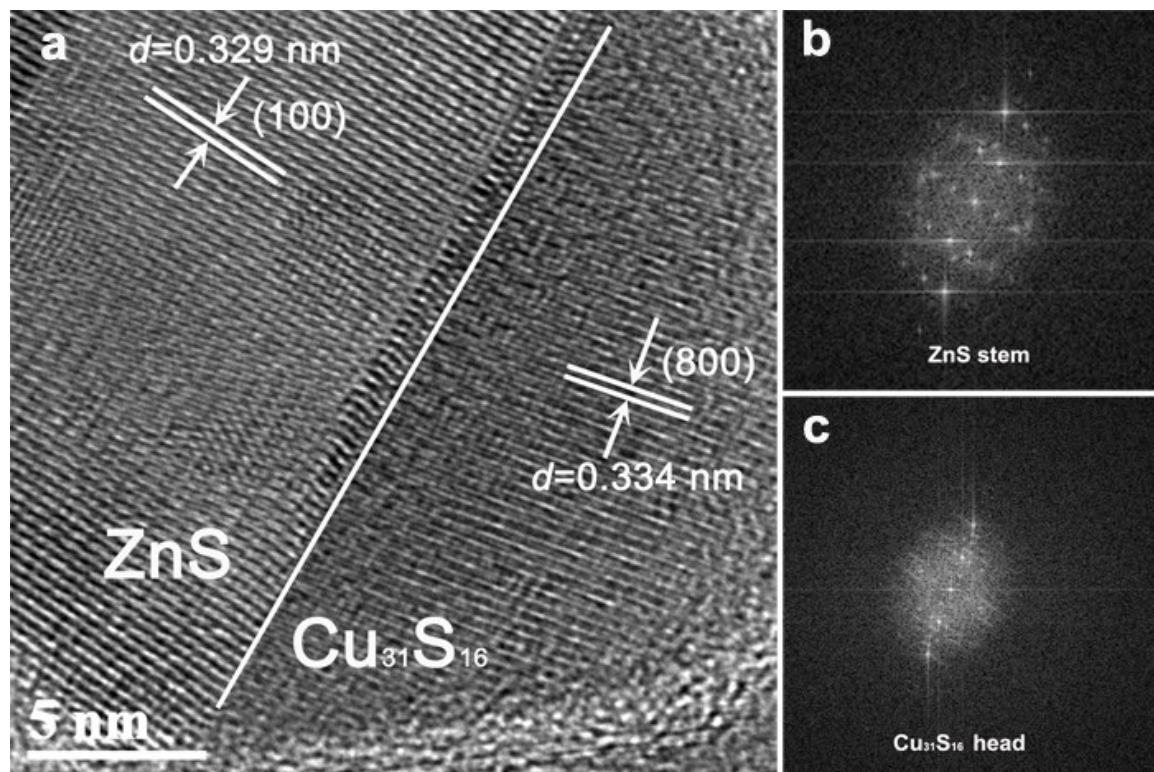


Fig.S1 (a) HRTEM image of a portion of a $\text{Cu}_{31}\text{S}_{16}$ -ZnS icecream-like HNS with different orientation, and the white long line is used to highlight the epitaxial boundary. (b, c) FFT patterns of the ZnS and $\text{Cu}_{31}\text{S}_{16}$ regions in Fig. 1a.

Figure. S2

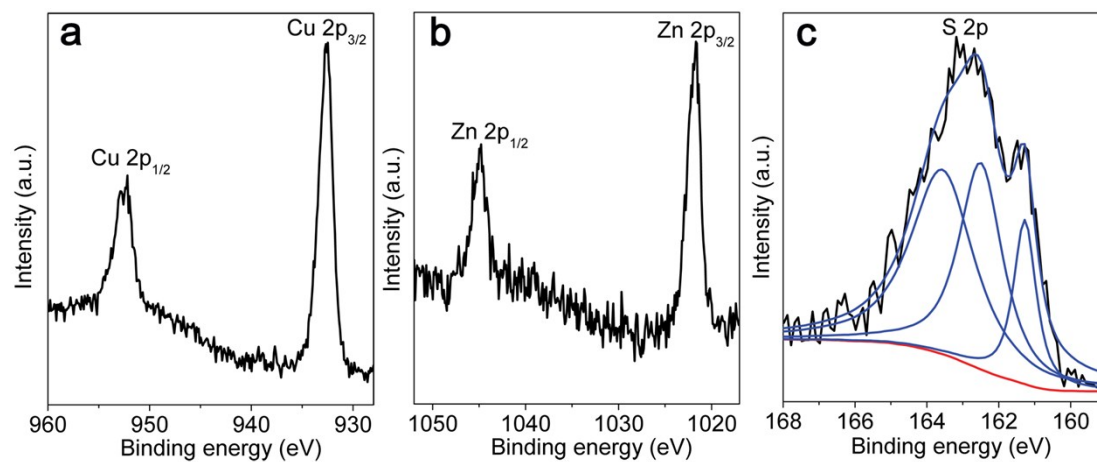


Fig.S2 High-resolution XPS spectra of icecream-like HNS: (a) Cu 2p; (b) Zn 2p and (c) S2p. Two symmetric peaks at 932.6 and 952.5 eV, and no satellite peaks are observed, which further confirms the presence of Cu(I) in the product.^{1,2} The Zn 2p peaks are located at 1044.9 and 1021.8 eV, and the peak splitting of 23.1 eV is consistent with the standard splitting of 22.97 eV, confirming the presence of Zn²⁺ in the icecream-like HNS.³ On the other hand, the S 2p can be fitted into three peaks, indicating the different chemical environment in terms of the formation of Cu-S and Zn-S bonds.

Figure. S3

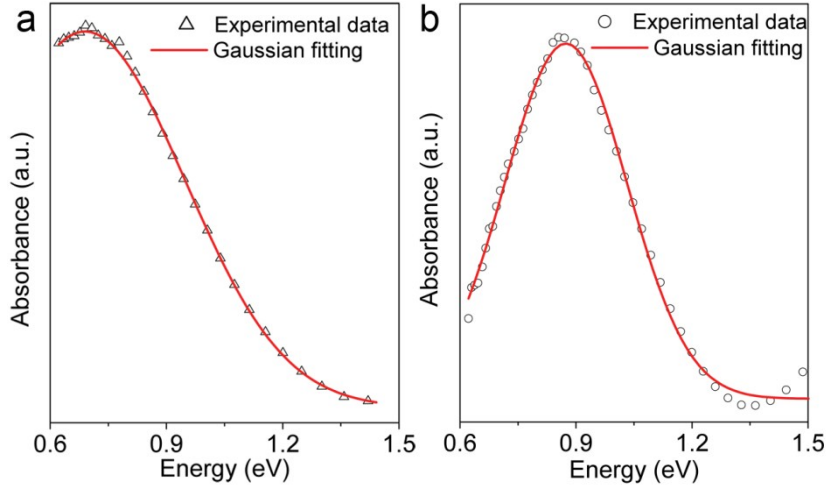


Fig.S3 Experimental (hollow scatters) and fitting results (red solid line) based on the Gaussian function of the LSPR spectra on the energy scale for different-shaped $\text{Cu}_{31}\text{S}_{16}\text{-ZnS}$ HNS synthesized by using different molar ratios of Cu/Zn sources: (a) Cu: Zn=1:1; (b) Cu:Zn=1:2. Herein, the morphology of the $\text{Cu}_{1.94}\text{S}$ head for different $\text{Cu}_{1.94}\text{S}$ -ZnS HNS is regarded as spheres, and the density of the carriers (holes) can be calculated based on Mie-Drude model, in which the LSPR frequency (ω_{sp}) is expressed as follows:⁴⁻⁶

$$\omega_{sp} = \sqrt{\frac{\omega_p^2}{1 + 2\varepsilon_m} - \gamma^2} \quad (1)$$

Where ε_m is the dielectric construction of the solvent, and $\varepsilon_m=4.8$ is available for the solvent chloroform at room temperature. γ is the full-width half at maximum (fwhm) of the plasmon resonance band, which can be obtained by fitting the absorption band to a Gaussian function. ω_p is the bulk plasmon oscillation frequency with expression

$$\omega_p = \sqrt{\frac{N_h e^2}{\varepsilon_0 m_h}} \quad (2)$$

where e is the electron charge, ε_0 is the free space permittivity, and m_h is the hole effective mass. As a result, the density of free holes can be calculated to be 5.5×10^{21} and $5.1 \times 10^{21} \text{ cm}^{-3}$ for icecream-like and mushroom-like $\text{Cu}_{31}\text{S}_{16}\text{-ZnS}$ HNS, respectively.

Figure. S4

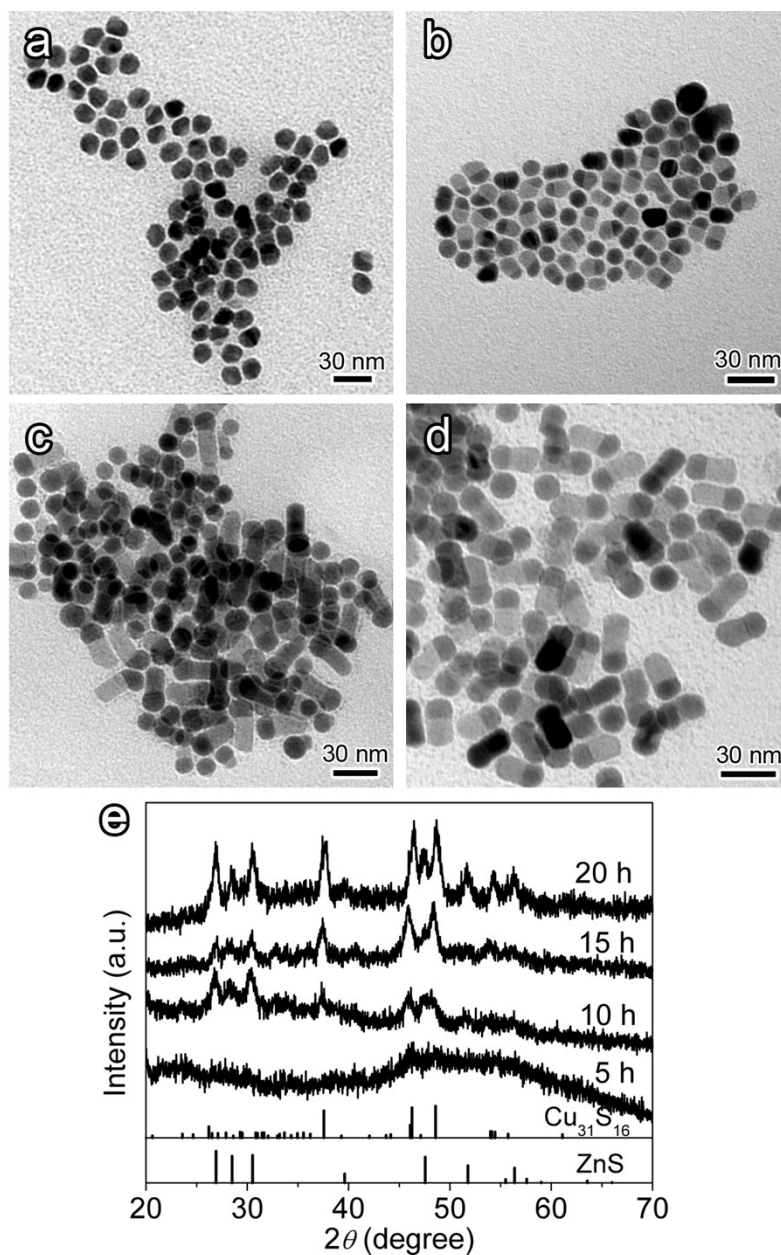


Fig.S4 TEM images of the short matchstick $\text{Cu}_{1.94}\text{S}$ -ZnS HNS (Cu:Zn=2:1) for different reaction time: (a) 5 h; (b) 10 h; (c) 15 h; (d) 20 h; and (e) the corresponding XRD patterns together with the standard diffraction lines of monoclinic $\text{Cu}_{31}\text{S}_{16}$ (JCPDS No.23-0959) and wurtzite ZnS (JCPDS No.36-1450) shown at the bottom. At the initial stage (5 h), the monoclinic $\text{Cu}_{31}\text{S}_{16}$ is the main phase, which can be confirmed by the TEM image and XRD patterns. The weak diffraction intensity may arise from the formation of gelatinoids, which is made up of the un-decomposed Cu-thiolate precursors, which was demonstrated in our previous work.⁷ As the reaction time is prolonged from 5 h to 20 h, a second phase appears on one side of the $\text{Cu}_{31}\text{S}_{16}$ phase and the length of the stick is increased from 8.9 ± 0.9 to 17.2 ± 2.2 nm. What's more, the diffraction intensity of the characteristic peak assigned to ZnS phase becomes stronger with the reaction time increasing, which also confirms the fraction of ZnS phase becomes larger.

Figure. S5

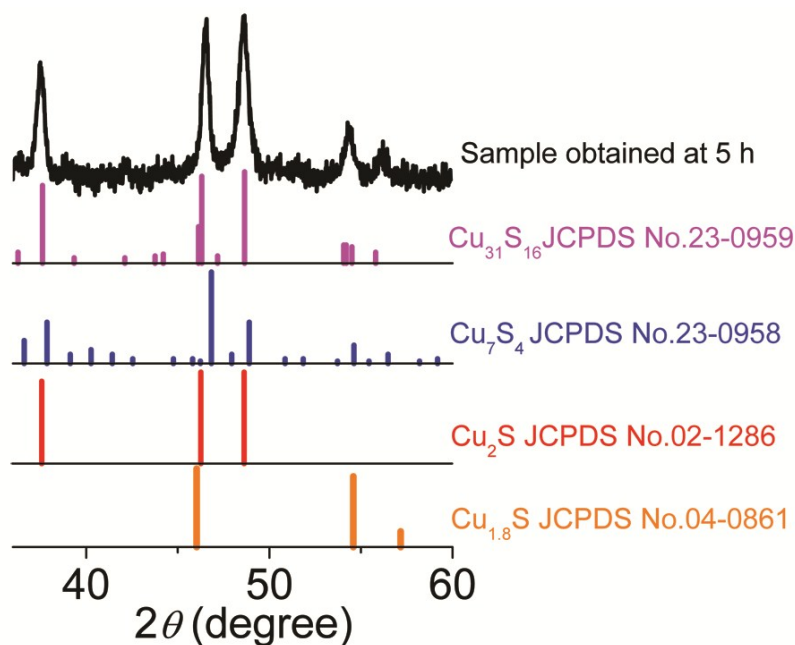


Fig.S5 XRD patterns of the sample synthesized without Zn precursors, and the bottom lines are the standard diffraction peaks of monoclinic $\text{Cu}_{31}\text{S}_{16}$ (djurleite, JCPDS No.23-0959), monoclinic Cu_7S_4 (roxbyite, JCPDS No. 23-0958), orthorhombic Cu_2S (α -chalcocite, JCPDS No.02-1286) and cubic $\text{Cu}_{1.8}\text{S}$ (digenite, JCPDS No.04-0861).The two diffraction peaks located at 46.5° and 48.6° match well with the $\text{Cu}_{31}\text{S}_{16}$ and Cu_2S , but the diffraction peak at 54.4° is absent in the Cu_2S , which indicates that the crystal structure of the sample can be assigned to monoclinic $\text{Cu}_{31}\text{S}_{16}$. Moreover, according to J.Kolny-Olesiak's work, the chalcocite nanocrystals are only stable under air-free conditions, which can undergo a phase transformation to djurleite phase.⁸ This further supports the formation of $\text{Cu}_{31}\text{S}_{16}$ nanocrystals.

Figure.S6

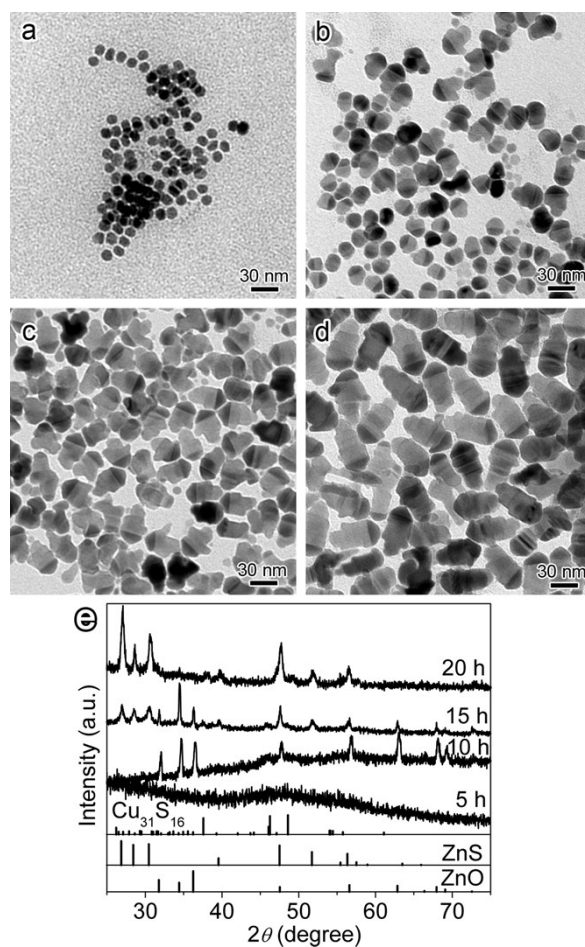


Fig.S6 TEM images of the icecream-like $\text{Cu}_{1.94}\text{S}$ -ZnS HNS (Cu:Zn=1:2) for different reaction time: (a) 5 h; (b) 10 h; (c) 15 h; (d) 20 h; and (e) the corresponding XRD patterns together with the standard diffraction lines of monoclinic $\text{Cu}_{31}\text{S}_{16}$ (JCPDS No.23-0959), wurtzite ZnS (JCPDS No.36-1450) and hexagonal ZnO (JCPDS No.36-1451) shown at the bottom. It can be seen from the XRD patterns that a broad but weak diffraction peak is observed in the product obtained at the initial stage (5 h), which may be assigned to monoclinic $\text{Cu}_{31}\text{S}_{16}$ phase in combination with the TEM results shown in Fig.S5a and our previous report. As the reaction time is prolonged to 10 h, a considerable fraction of ZnO phase together with some non-negligible and weak $\text{Cu}_{31}\text{S}_{16}$ phase are observed in the XRD result, and the formation of ZnO phase can be attributed to the reaction between Zn sources with the oxygen in the reaction system.² Further increasing reaction time to 15 h leads to a decrease in the diffraction intensity of ZnO phase and an increase in the diffraction intensity of a new phase assigned to wurtzite ZnS phase. Finally, the wurtzite ZnS phase dominates over the XRD patterns of the products obtained at 20 h, but the weak diffraction peaks indexed as $\text{Cu}_{31}\text{S}_{16}$ is also detected, indicating the formation of $\text{Cu}_{31}\text{S}_{16}$ -ZnS HNS. Accordingly, the mean stick length of the icecream-like $\text{Cu}_{31}\text{S}_{16}$ -ZnS HNS is increased from 20.1 ± 2.5 nm (10 h) to 44.7 ± 3.6 nm (20 h), and the mean diameter of the head is also increased from 11.6 ± 0.9 nm (5 h) to 26.0 ± 2.1 nm (20 h), indicating the fraction of ZnS phase becomes larger in the HNS with longer

reaction time (Fig.S5d).

Figure. S7

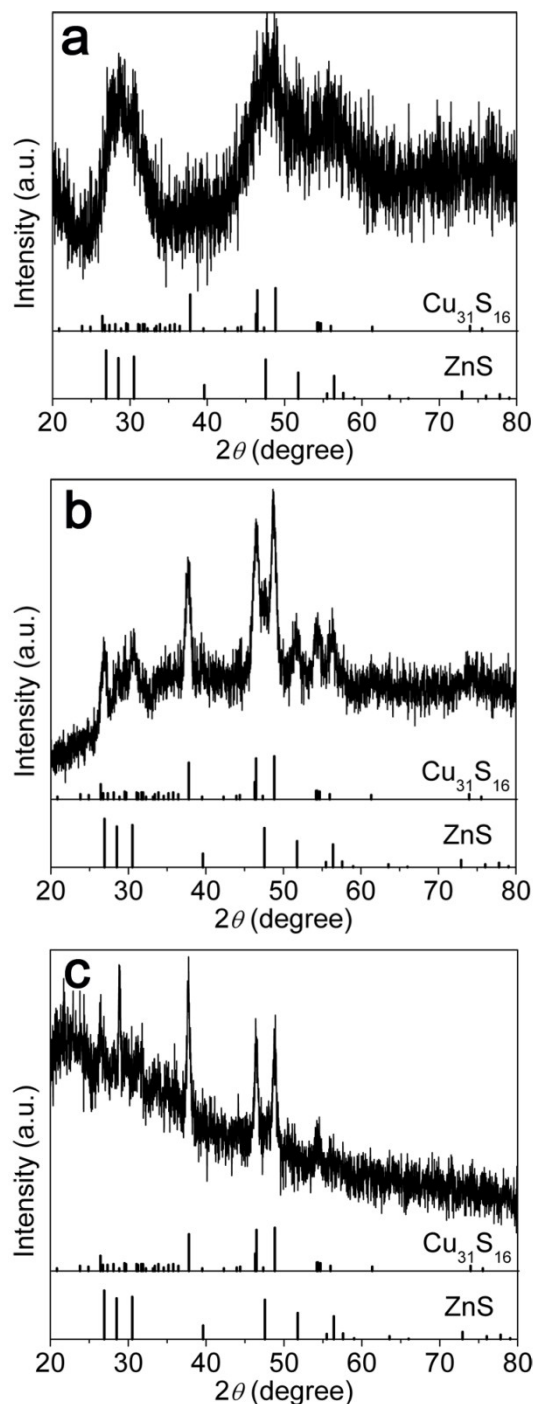


Fig.S7 XRD patterns of different $\text{Cu}_{31}\text{S}_{16}$ -ZnS HNS synthesized by using different Zn sources:(a) $\text{Zn}(\text{OAc})_2$; (b) ZnSO_4 ; (c) ZnCl_2 ; The bottom lines represent the standard diffraction peaks of monoclinic $\text{Cu}_{31}\text{S}_{16}$ (JCPDS No.23-0959) and wurtzite ZnS (JCPDS No.36-1450).

Figure. S8

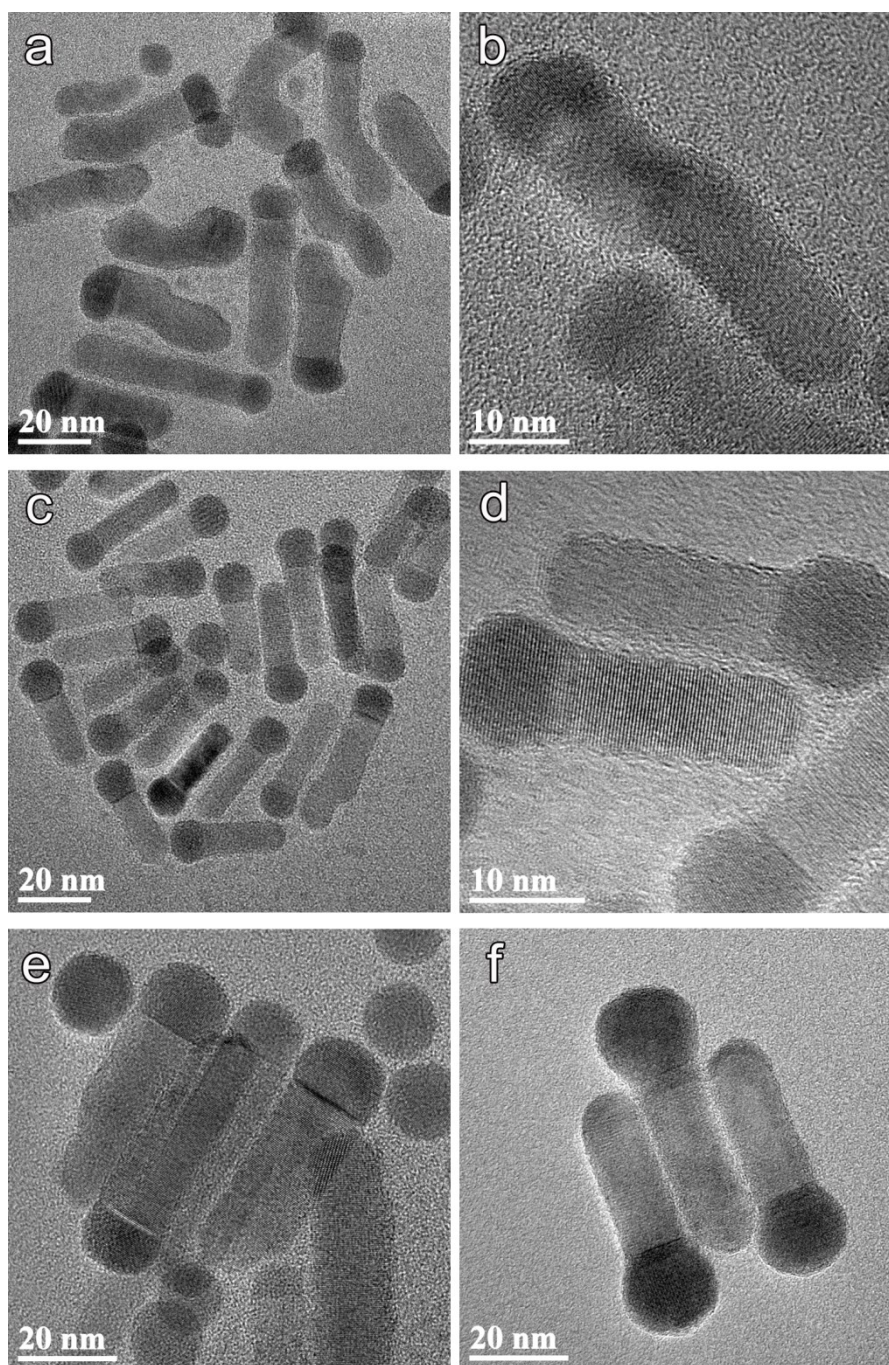


Fig.S8 HRTEM images of different-shaped Cu₃₁S₁₆-ZnS HNS synthesized by using different Zn sources:(a, b) Zn(OAc)₂; (c,d) ZnSO₄; (e,f) ZnCl₂.

Figure. S9

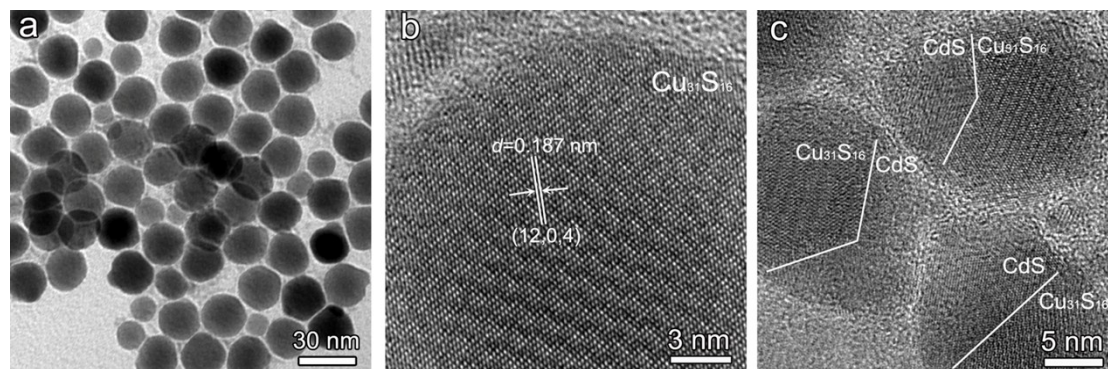


Fig.S9 (a) Low-magnified TEM image of the as-obtained sample composed of $\text{Cu}_{31}\text{S}_{16}$ -CdS HNS and some isolated $\text{Cu}_{31}\text{S}_{16}$ nanocrystals; (b) HRTEM image of $\text{Cu}_{31}\text{S}_{16}$ and (c) HRTEM image of HNS.

Figure. S10

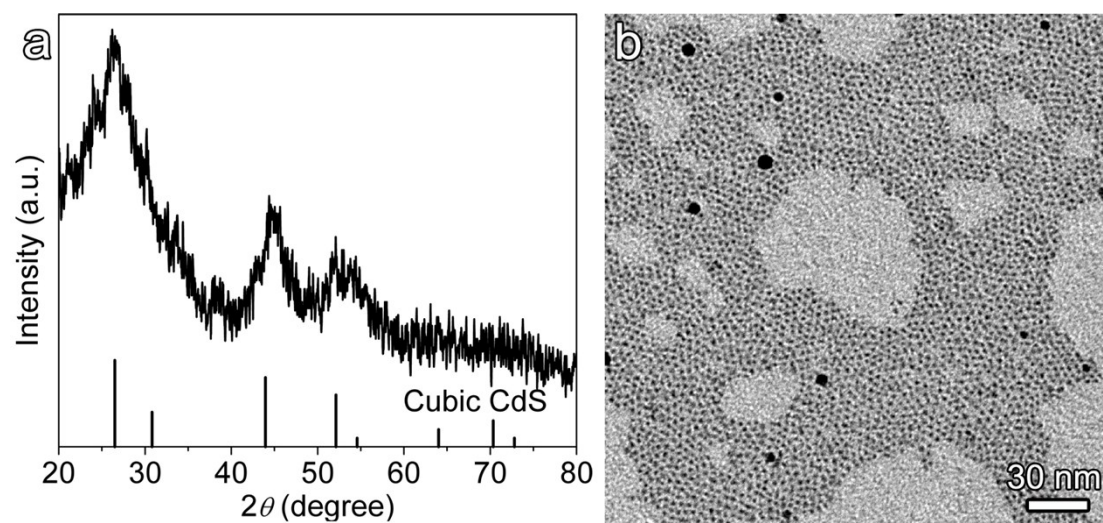


Fig.S10 (a) XRD patterns of CdS:Cu(I) synthesized by using Cu/Cd precursor ratio being 2:3, and the bottom lines are the standard diffraction peaks of cubic CdS (JCPDS 10-0454); (b) the corresponding TEM image.

Figure. 11

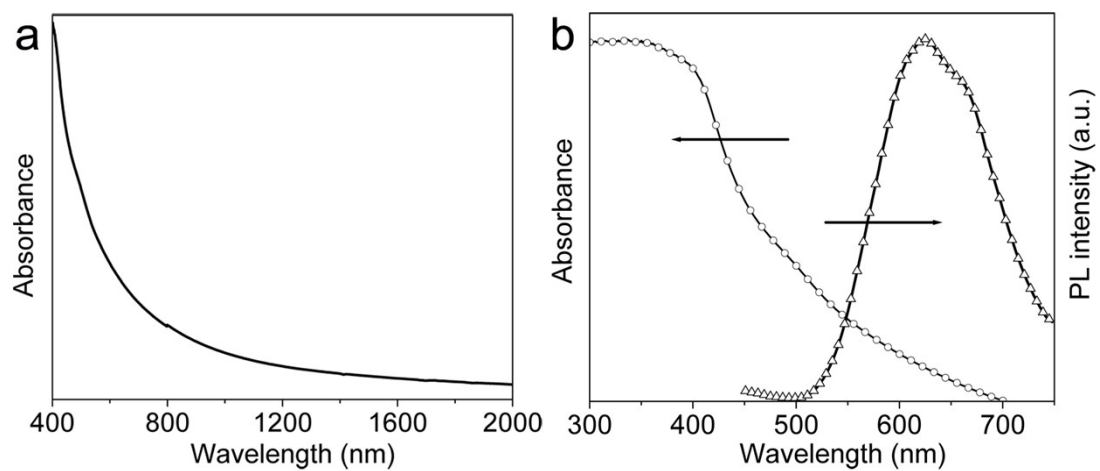


Fig.S11 (a) Vis-NIR absorption spectrum and (b) UV-Vis absorption and PL spectra of CdS:Cu(I) synthesized by using Cu/Cd precursor ratio being 2:3.

Figure. S12

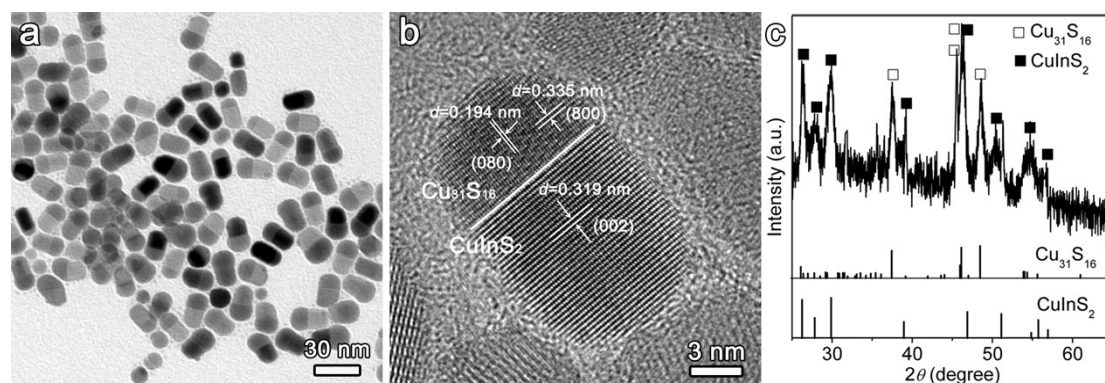


Fig.12 (a) TEM image and (b) HRTEM image of $\text{Cu}_{31}\text{S}_{16}$ - CuInS_2 HNS synthesized by using the Cu/In precursor ratio of 1:1. The analysis of the lattice fringes in HRTEM images reveals that the (800) planes ($d=0.336$ nm) of monoclinic $\text{Cu}_{31}\text{S}_{16}$ phase is coincident with the (002) planes of wurtzite CuInS_2 phase. (c) XRD patterns of $\text{Cu}_{31}\text{S}_{16}$ - CuInS_2 HNS, and the bottom lines represent the standard diffraction lines of monoclinic $\text{Cu}_{31}\text{S}_{16}$ and wurtzite CuInS_2 phase. The aforementioned results indicate that the HNS are indeed composed of $\text{Cu}_{31}\text{S}_{16}$ and CuInS_2 . This two-phase strategy may shed light on the synthesis of $\text{Cu}_{31}\text{S}_{16}$ -based HNS with controllable shape and composition.

Figure. S13

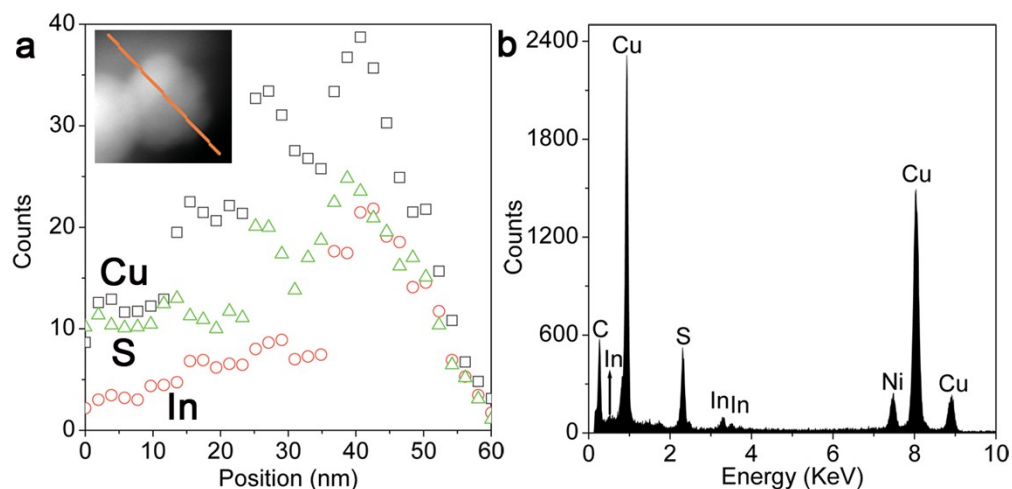


Fig.13 (a) Elemental profiles of Cu (square hollows), In (spherical hollows) and S (triangular hollows) measured by using line-scanned EDX spectra, and the inset shows the dark-field scanning TEM image; (b) EDX spectrum of $\text{Cu}_{31}\text{S}_{16}$ - CuInS_2 HNS synthesized by using the Cu/In precursor ratio of 1:1. The elemental profiles shown in Fig.12(a) demonstrate that the content of Cu and S is dispersed throughout the whole HNS, and the In is limited to the stem part of HNS, which further confirms the formation of $\text{Cu}_{31}\text{S}_{16}$ - CuInS_2 HNS. As a matter of fact, the $\text{Cu}_{1.94}\text{S}$ - CuInS_2 HNS have been synthesized by other colloidal approaches, which is an essential intermediate step in the growth of ternary CuInS_2 nanocrystals.⁸⁻¹⁰

References

1. H. Ye, A. Tang, C. Yang, K. Li, Y. Hou and F. Teng, *CrystEngComm.*, 2014, 16, 8684-8690.
2. M. Wang, A. W. Tang, D. X. Zhu, C. H. Yang and F. Teng, *CrystEngComm.*, 2015, 17, 6598-6606.
3. Z. Y. Liu, A. W. Tang, M. Wang, C. H. Yang, and F. Teng, *J. Mater. Chem. C*, 2015, 3, 10114-10120.
4. Y. Xie, L. Carbone, C. Nobile, V. Grillo, S. D'Agostino, F. D. Sala, C. Giannini, D. Altamura, C. Oelsner, C. Krysch and P. D. Cozzoli, *ACS Nano.*, 2013, 7, 7352-7369.
5. A. Comin and L. Manna, *Chem. Soc. Rev.*, 2014, 43, 3957-3975.
6. J. M. Luther, P. K. Jaiih, T. Ewers and A. P. Alivisatos, *Nat.Mater.*, 2011, 10, 361-364.
7. A. W. Tang, S. C. Qu, K. Li, Y. B. Hou, F. Teng, J. Cao, Y. S. Wang and Z. G. Wang, *Nanotechnology*, 2010, 21, 285602.
8. J. Li, M. Bloemen, J. Parisi and J. Kolny-Olesiak, *ACS Appl. Mater. Interfaces.*, 2014, 6, 20535-20543. (c) M. Kruszynska, H. Borchert, J. Parisi and J. Kolny-Olesiak, *J. Am. Chem. Soc.* 2010, 132, 15976-15986.
9. J. Li, M. Bloemen, J. Parisi and J. Kolny-Olesiak, *ACS Appl. Mater. Interfaces*, 2014, 6, 20535-20543.
10. S. T. Connor, C-M. Hsu, B. D. Weil, S. Aloni and Y. Cui, *J. Am. Chem. Soc.*, 2009, 131, 4962-4966.